JOURNAL OF SPACECRAFT AND ROCKETS
Vol. 48, No. 1, January–February 2011

Erosion of Carbon-Based Materials Under High-Fluence Heavy-Ion Irradiation

N. N. Andrianova,* A. M. Borisov,† and E. S. Mashkova†
Moscow State University, 119991, Moscow, Russia
and
Yu. S. Virgiliev‡
NIIgraphite, 111141, Moscow, Russia

DOI: 10.2514/1.49462

The sputtering, morphology, and crystalline structure modification of highly oriented pyrolytic graphite, polycrystalline graphites, glassy carbons, and the carbon-fiber composite materials under high-fluence (10^{18}–10^{19} ion/cm^2) 30 keV N_2^+ and Ar^+ ions at the incidence angles from 0° (normal incidence) to 80° from room temperature till elevated temperatures (∼400°C) have been studied. The radiation damage influence on the erosion regularities is discussed.

Nomenclature

T	=	target temperature, °C
T_a	=	dynamic annealing temperature of radiation damage, °C
T_t	=	temperature of texture transition, °C
Y	=	sputtering yield, atoms/ion
γ	=	ion-induced electron emission yield, electron/ion
θ	=	angle of ion incidence, deg
λ	=	mean path length of secondary electrons, nm
φt	=	irradiation fluence, ion/cm^2

Subscripts

a	=	annealing
t	=	texture

I. Introduction

EXTENSIVE investigations on the interaction of the various environmental species with spacecraft materials are conducted in both in-flight and ground-based testing experiments for the analysis of the materials' radiation durability and modification. There are many forms of radiation in space. Among them, the irradiation may be created by Earth's hot magnetosphere plasma with a typical heavy-ion energy range of 10^3–10^5 eV. Radiation damage created by ion irradiation (and also by secondary neutrons) is due to the material atom displacements as a result of energy transferred in practically elastic collisions in a cascade effect. The changes of physical and functional properties of the spacecraft materials and, accordingly, the radiation protection of such materials remain a main challenge in connection with the preparation of new space projects such as the construction of the moon stations and the flights to Mars and Jupiter. On long flights lasting many years, the irradiation fluences may be larger than $\sim 10^{17}$ cm^{-1}.

In the aerospace industry, the carbon-based materials are widely used due to their strength, heat shielding properties, and a number of other specific characteristics [1]. These materials often stand out as an individual class of materials in the study of mechanisms of radiation damage and their effect on physical properties of solids [2,3]. Virtually all types of radiation influence lead to temperature-dependent structural changes of carbon-based materials, such as changes in crystal lattice parameters, concentration of defects, and surface-topography evolution. Primary radiation defects in a graphite crystal lattice (namely, displaced atoms and vacancies) are caused (as in other solids) by a cascade mechanism of atomic displacements as a result of primary high-energy particles (neutrons, ions, fission fragments, etc.) stopping in material. Displaced atoms and vacancies partially recombine or remain in the form of point defects or form more complex defects (clusters of displaced atoms and vacancies), depending on the target temperature at which irradiation occurs. One part of displaced atoms recombines with vacancies; another part forms linear molecules C_2, C_3, and C_4, which can in turn form the dislocation loops: new graphite planes. As a result, graphite crystallites can grow along the c axis (Fig. 1). Relaxation in graphite atomic planes due to vacancy coalescence results in a decrease in crystallite sizes in a basal plane [3]. For the carbon-based materials, significant effects of radiation damage are observed at temperatures close to room temperature (RT): i.e., in the region where the majority of radiation defects in metals are practically annealed. With increasing temperature, radiation-defect mobility results in the complex processes of dynamic annealing [3,4]. The ion-induced kinetic processes controlling surface evolution (erosion) are mainly the sputtering and the defect-diffusion processes [5,6]. By now, sufficiently detailed data have been accumulated about physical and chemical sputtering of carbon-based materials used in thermonuclear devices under the light ions (hydrogen and helium isotopes) and C^+ and O^+ ions and the data about erosion of the spacecraft and rocket materials under oxygen ions and atoms [7,8]. The interactions of rather heavy ions (in particular, nitrogen ions and inert gas ions with carbon-based materials) have been insufficiently investigated.

In the aerospace industry, carbon–carbon composite materials consisting of reinforcing carbon fibers embedded in carbon or graphite matrix, named carbon-fiber composites (CFCs), are widely used. The structure of the CFC basic element, namely, carbon fibers, represents an imperfect kernel with a turbostrate structure and a highly perfect textured shell. A shell is formed by the graphite layers oriented in a parallel to the fiber surface, so that the c-crystallographic axis is directed along the fiber radius. A CFC reinforcing skeleton is subjected to impregnation procedure and/or pyrolysis. As a result, the matrix consists of both isotropic carbon-based materials (pitches, resins, and pyrocarbon) and anisotropic materials (pyrographite) and combinations thereof. Thermal stabilization of CFC under high-temperature (up to ∼2500°C) heat treatment results in graphitization of pitch and pyrocarbon in the matrix and weakly graphitized polymer binding agents remain in a

Received 19 February 2010; revision received 25 June 2010; accepted for publication 8 September 2010.

*Senior Research Scientist, Institute of Nuclear Physics.
†Leading Research Scientist, Institute of Nuclear Physics.
‡Principal Research Scientist.

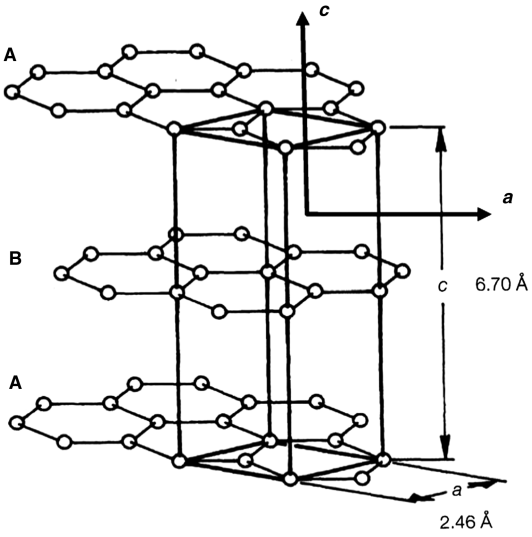

Fig. 1 Crystal lattice of graphite.

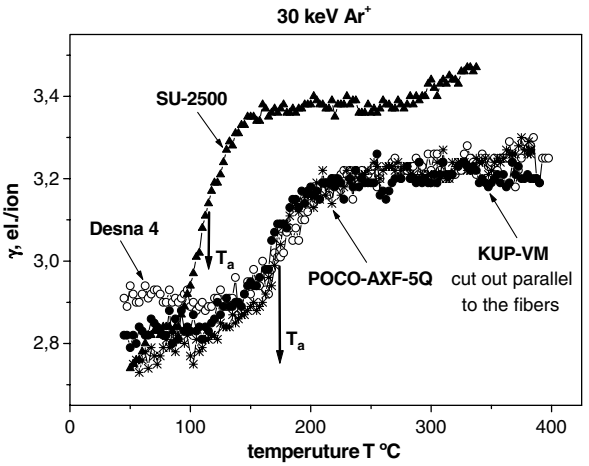

Fig. 2 Temperature dependences of γ at normal incidence of Ar^+ ions.

turbostrate form. The degree of crystal structure perfection of a matrix substantially defines the rate and level of radiation changes of material properties [1].

The aim of the present work is the investigations of the regularities of high-fluence heavy-ion irradiation of carbon-based materials, including the temperature and angular dependences of sputtering: i.e., ejection of carbon atoms from the surface with the consequent surface erosion, namely, with the structure and morphology changes of the modified surface layers.

II. Experimental

The experiments have been carried out on the mass-monochromator of the Institute of Nuclear Physics, Moscow State University [9]. The 5–35 keV ion beam was produced in arc source with a longitudinal magnetic field. The ions were separated and the beam was focused by a Siegban-type magnetic sector field. The experimental procedure is described elsewhere [10]. The target holder permitted the variation of the angle θ of ion incidence from 0 to 89° and of the target temperature from −180 to 1000°C. The samples for the investigation were commercial carbon-based materials: polygranular graphite POCO-AXF-5Q (U.S.-produced) and polygranular graphite MPG-8, highly oriented pyrolytic graphite (HOPG) UPV-1T, glassy carbons, and the CFCs (all NIIgraphite-produced). CFC KUP-VM (1-D) is based on VMN-4 polyacrylonitrile (PAN) fibers, and Desna 4 (4-D) reinforced composite is also based on PAN fibers (UKN-5000), with a matrix prepared via multiple pitch-impregnation cycles. The samples had the shape of rectangular plates. A polycrystalline copper target was also used for comparison. Vacuum annealing (usually at $T \geq 250$°C) of carbon materials is necessary because of their sorption properties. The irradiation was produced by 30 keV Ar^+ and N_2^+ ions, ion current was ∼0.4 mA/cm^2, the cross section of ion beam was 0.3 cm^2. The total ion fluences were 10^{18}–10^{19} ion/cm^2. The ion-induced electron emission yield γ was determined as the ratio of the electron current to the primary ion current with the instrument error ∼2.5%. The target bias (−250 V) with respect to a surrounding collector (Faraday cup) conforms to electron current saturation. Sputtering yields Y were determined by weight-loss measurements. The error of the measured yield Y was estimated to be 15%, mainly due to the necessity to take into account gas adsorption.

Investigations of the samples before and after irradiation included analysis of surface topography by scanning electron microscopy (SEM) using LEO-1430vp, scanning probe microscope FemtoScan in atomic force microscopy (AFM) mode, optical microscope Axiostar Plus, and the laser goniophotometry (LGP) technique [11]. The elemental analysis was carried out by Rutherford backscattering (RBS) using 2 MeV He^+ ions. The structure analysis was made using reflection high-energy electron diffraction (RHEED) in EMR-102 (Russian model) operated at 50 kV and electron beam current of 50 μA.

III. Computer Simulation

Computer simulation of sputtering was carried out by Eckstein [12] using the program TRIM.SP (version trvmc 95), which simulates only the low-fluence or equilibrium case when elemental composition and other target parameters do not change. To describe collisions of a bombarding ion with target atoms and target atoms between themselves, the potential Wilson–Haggmark–Biersack (Kr–C) with the Firsov screening length was used. The graphite target density was taken equal either to the theoretical density (2.26 g/cm^3) or equal to the real density of the used materials. The target (irradiated by 30 keV N_2^+) was assumed to contain nitrogen and oxygen in addition to carbon in the ratio taken from the analysis of the experimentally obtained RBS spectra (C:N:O = 77:19:4). The binding energy of component atoms was taken equal to 7.4 eV (the tabular value of the graphite sublimation energy). Inelastic energy losses were taken into account in equal ratios according to the Lindhard–Sharff and Oen–Robinson models. Statistics of bombarding particles were 0.5–2 × 10^6, depending on the simulated situation. To study the effect of the target surface topography developing under ion irradiation, the distributions of local slope angles of ion incidence onto the faces of topographic elements were measured using LGP. The estimates according to [13] show that the dynamic steady-state conditions in the considered experiments occur at the fluences of the order of 10^{17}–10^{18} ion/cm^2. In this case the level of radiation damage determined by a number of displacement per atom (dpa) can reach values on the order of 10^2. Some estimates were carried out using code SRIM-2008.[§]

IV. Results and Discussion

Analysis of the experimental data on sputtering and ion-induced electron emission shows that the dynamically equilibrium state of the graphite surface, characterized by stabilization of the yields of sputtering Y and ion-induced electron emission γ and by the specific developed surface morphology, occurs at the irradiation fluences of 10^{18}–10^{19} ion/cm^2. The regions of the different behaviors of studied characteristics are separated by the dynamic annealing temperature T_a of radiation damage, determined by a steplike behavior of a temperature dependence of ion-induced electron emission yield γ [14]. The value of T_a depends on the given carbon-based material (see Fig. 2). The γ jump has been explained by the dependence of a mean path length λ of the secondary electrons on changes in the lattice structure. Namely, it is connected with a transition from a strongly disordered surface layer under ion irradiation at $T < T_a$ to a polycrystalline phase at $T > T_a$ [14]. As a result, in situ monitoring of

[§]Data available online at http:/www.srim.org [retrieved June 2008].

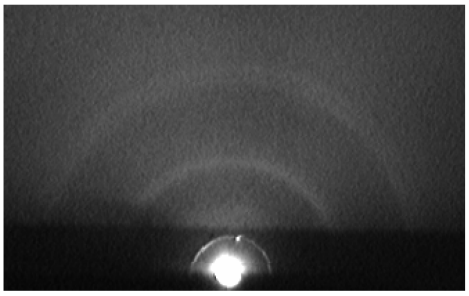

a)

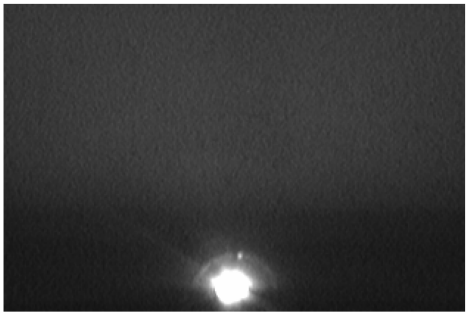

b)

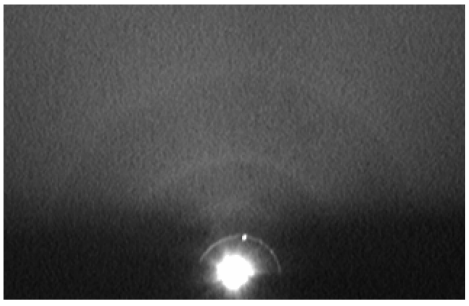

c)

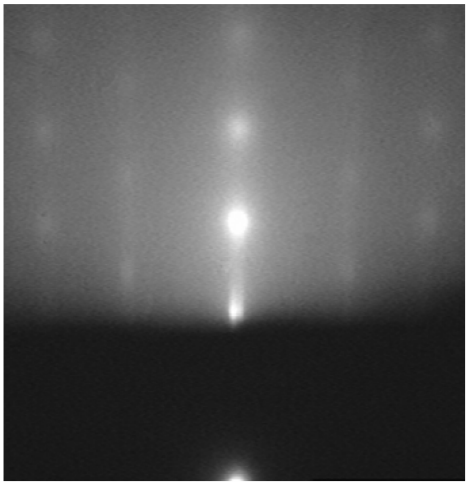

d)

Fig. 3 RHEED patterns of CFC (KUP-VM) samples cut out parallel to the fibers a) before and after 30 keV N_2^+ ion irradiation at normal incidence: b) RT, c) $T = 350°C$, and d) initial HOPG (UPV-1T).

structural changes of carbon-based materials under ion irradiation has been provided by ion-induced electron emission.

A. Structure and Topographical Changes

For the native, both isotropic graphites and CFC RHEED show three rings (see Fig. 3a). Under ion irradiation at $T < T_a$, the diffraction patterns show a high degree of disorder (diffuse halo) (Fig. 3b). At elevated temperatures ($T > T_a$), the patterns have been found to be similar to those for the nonirradiated surfaces (see Fig. 3c).

It is known that the polycrystalline artificial graphite microstructure is porous, with porosity up to 20%, and contains graphitized crystalline particles (different in shape) and the fragments of weakly graphitized coupling carbon [3]. High-fluence irradiation with heavy ions results in the disappearance of the flaky virgin-surface structure, a strong increase in total roughness, and the appearance of the cone systems whose axes directions coincide with the direction of incidence of the ion beam [10]. The cone-shaped formations and column-inclined structures with conical vertices are the main elements of a developed morphology in a dynamic steady state. Evolution of a surface morphology depends on target temperature, angle of ion incidence θ, and a type of carbon-based material. Note that the dynamic steady-state surface morphology of graphites with similar topographic elements has been observed under both argon and nitrogen ion irradiation. It is usually a consequence of physical sputtering with relatively heavy ions of a nonuniform surface of random solids, following the erosion theories [5,6,15].

The investigation of highly oriented pyrolytic graphite samples (UPV-1T) also showed the difference in the surface structure and developed morphology for different irradiation temperatures and angles of ion incidence. The difference is more complex than under similar irradiation conditions for polycrystalline graphites. In contrast to polycrystalline graphites, the basal plane (0001) of UPV-1T can be considered to be virtually smooth. The SEM investigations of the samples after irradiation by 30 keV N_2^+ ions at normal ion incidence and the temperatures close to RT show that a system of the craters with smooth and gently sloping walls (with a distance of 0.5–1 μm between them) appears at the UPV-1T surface (see Fig. 4a). The difference between the topography developing under irradiation at RT and $T > T_a$ increases for oblique ion incidence. Namely, a faceted structure develops at room temperature [see SEM-data (Fig. 4b) and at three-dimensional reconstruction of surface morphology using AFM (Fig. 4c)], whereas a system of specific accreted needle-shaped cones is created at $T > T_a$ (Fig. 4d). RHEED shows that nonirradiated basal plane (0001) of HOPG (UPV-1T) contains the 002*l*-type point reflections, corresponding to a graphite single crystal with the *c*-axis orientation close to normal to the sample surface (see Fig. 3d). After ion irradiation at RT, the appearance of an amorphous halo in the electron diffraction patterns for both normal and oblique ion incidence indicates strong crystal structure disordering. The diffraction patterns for the samples irradiated at elevated temperatures differ from the virgin sample pattern and from the case of irradiation at RT and, in addition, strongly depend on the angle of incidence and the measurement geometry of an electron diffraction pattern. For normal ion incidence and for incidence close to the normal one, three diffuse rings corresponding to the three most intense rings in the electron diffraction patterns of polycrystalline graphites are observed. Taking into account the formation of needlelike topographic elements at oblique ion incidence (Fig. 4d), it is obviously that different faces of the developed topographical elements are irradiated at substantially different local angles of ion incidence. The butt ends of the topographic elements are irradiated at ion incidence close to the normal one. When the structures of upper gently sloping faces were analyzed, ring families of point reflections of graphite prismatic planes were observed, which indicates a change in the highly oriented pyrolytic graphite origin texture, probably caused by graphite crystallite twinning under ion bombardment [16]. The greatest restoration of the material origin structure after continuous irradiation at elevated target temperatures is observed at a grazing irradiation. It correlates with a decrease of *dpa* more than an order of magnitude at the grazing incidence of ions onto a target, as compared to the normal incidence of ions [13]. A crystalline structure of UPV-1T basal plane at elevated temperatures and oblique ion incidence is more ordered than in the case of RT irradiation. Under high-fluence irradiation of ordered solids, the diffusion processes are very important. Namely, a diffusion of the surface atoms is not isotropic and results in strong and complex dependence of surface morphology on an irradiation temperature [6]. As a result, the height of the

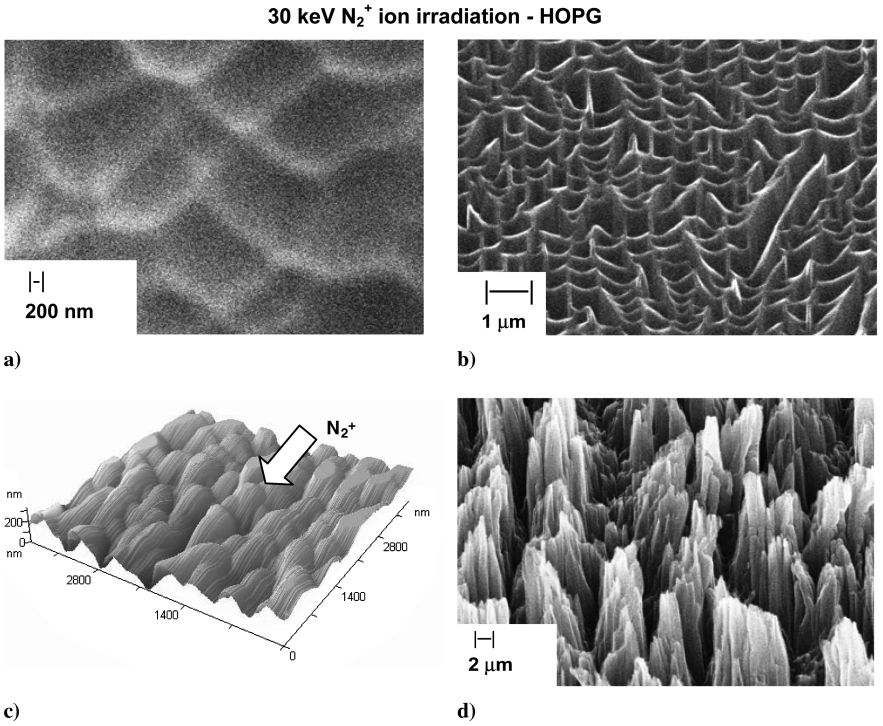

Fig. 4 SEM micrographs of HOPG (UPV-1T): a) $\theta = 0°$, RT; b) $\theta = 60°$, RT; c) three-dimensional reconstruction using AFM; and d) $\theta = 60°$; $T = 400°C$.

created topographical elements may be large, demonstrating the diffusion processes in a morphological formation. The height of needle-shaped topographical elements presented in Fig. 4d is $\sim$10 μm. This height is much more than the thickness of the sputtered layer, which is about 1 μm. Topography evolution under 30 keV Ar^+ irradiation, as in the 30 keV N_2^+ case, appreciably differs from the topography developing for random carbon-based materials. In addition, in the case of Ar^+ irradiation, there is practically no difference between the topography developed at RT and elevated temperatures ($T > T_a$) (see Fig. 5a). In both cases, two main components can be distinguished: the walls of needle-shaped elements directed toward the ion beam direction and the porous microfaces faced to the ion beam (Fig. 5b).

The glassy-carbon (SU-850 and SU-2000) surface topography developing under ion bombardment showed substantial differences for low- and high-temperature glassy carbons irradiated at $T < T_a$ (see Fig. 6). The glassy carbons SU-850, SU-2000, and SU-2500 are distinguished by the temperature of heat treatment: namely, 850, 2000, and 2500°C. SU-850 is a low-temperature glassy carbon, and SU-2000 and SU-2500 are the high-temperature glassy carbons. For high-temperature glassy carbons, some shallow etch pits with pentagonal and hexagonal forms have been observed, whereas for low-temperature glassy carbons, there are also deeper polygonal pits. At elevated temperatures for all studied glassy carbons, some ridges with steep walls are developed [17].

The problems of erosion and modification of the structure and morphology of the CFC surface layer under light-ion irradiation (hydrogen and helium isotopes) are the subject of intense investigation in connection with the solution of material science problems of the International Thermonuclear Experimental Reactor [18,19]. Erosion of the CFC under irradiation with oxygen ions and atoms has been investigated intensely to simulate the effect of factors of space environment on materials of spacecraft [20]. The studies of heavy-ion irradiation influence on a structure and the properties of the carbon fibers show the radiation-induced modification of a fiber morphology [19,21,22]. In our studies of high-fluence ion irradiation of CFC materials, as for other carbon-based materials, the temperature dependences of ion-induced electron emission were used for in situ monitoring of the ion-induced structure changes. The temperature dependences $\gamma(T)$ presented in Fig. 2 for both KUP-VM (1-D) and Desna 4 (4-D) demonstrate a steplike increase (jump) of ion-induced electron emission yield γ at a dynamic annealing temperature T_a. In the studied case of Ar^+ ion irradiation $T_a \approx$ 170°C, it is close to the corresponding value for polycrystalline graphite POCO-AXF-5Q. The fiber morphology changes depend strongly on the temperature at which irradiation is carried out. At

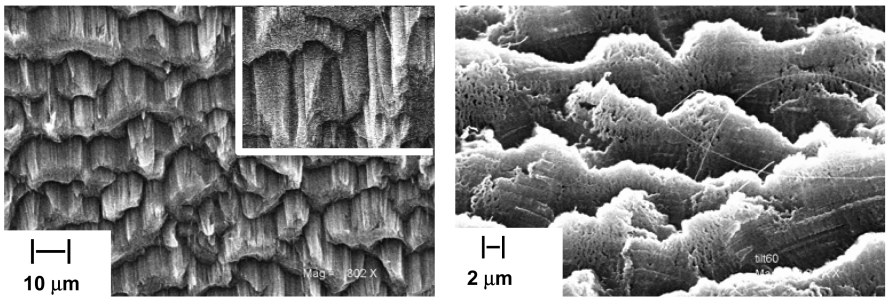

Fig. 5 SEM micrographs of UPV-1T surface after 30 keV Ar^+ ion irradiation: a) $\theta = 60°$, $T = 400°C$, inset at RT, and tilt 30° and b) $\theta = 60°$, $T = 400°C$, and tilt 60° (i.e., electron probing direction coincides with ion beam direction); $\varphi t \sim 10^{20}$ ion/cm^2.

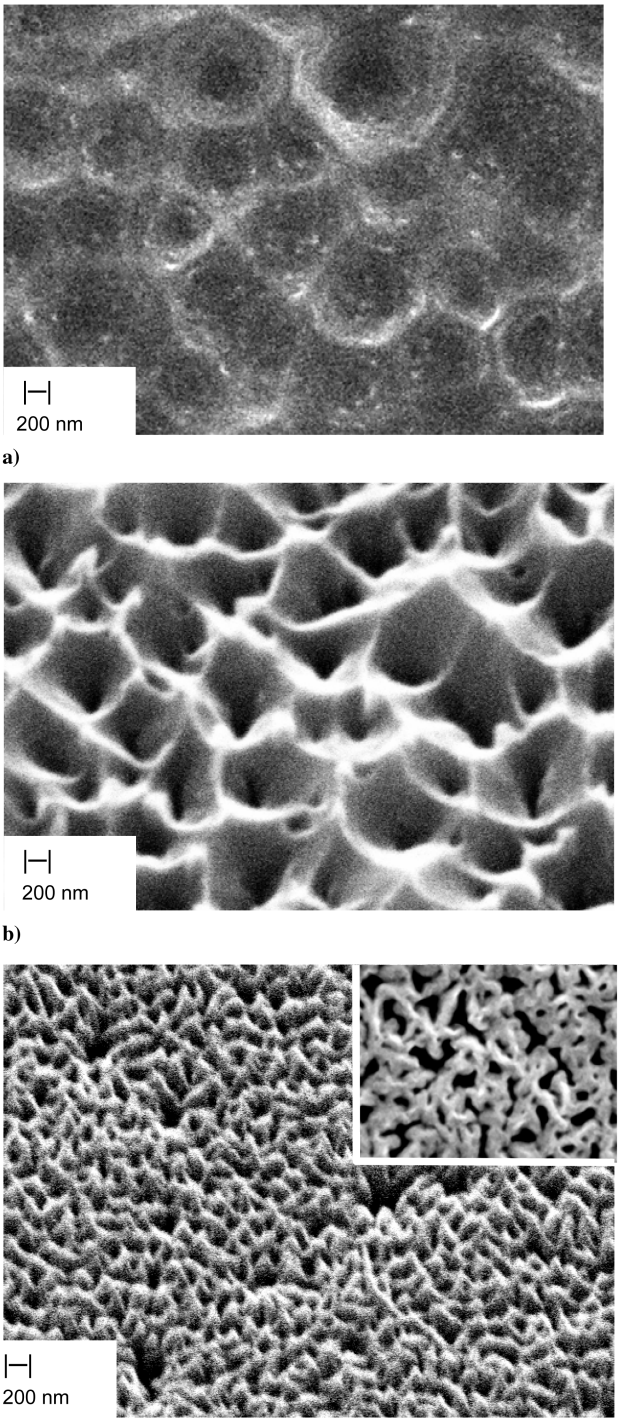

Fig. 6 SEM micrographs of glassy-carbon surface after irradiation: a) 30 keV N_2^+ SU-2000, RT, and tilt 0, b) 30 keV N_2^+ SU-850, RT, and tilt 30°, c) 30 keV Ar^+ SU-850, $T = 300$°C, and tilt 30° (tilt 0 in the inset); $\varphi t \sim 10^{19}$ ion/cm^2.

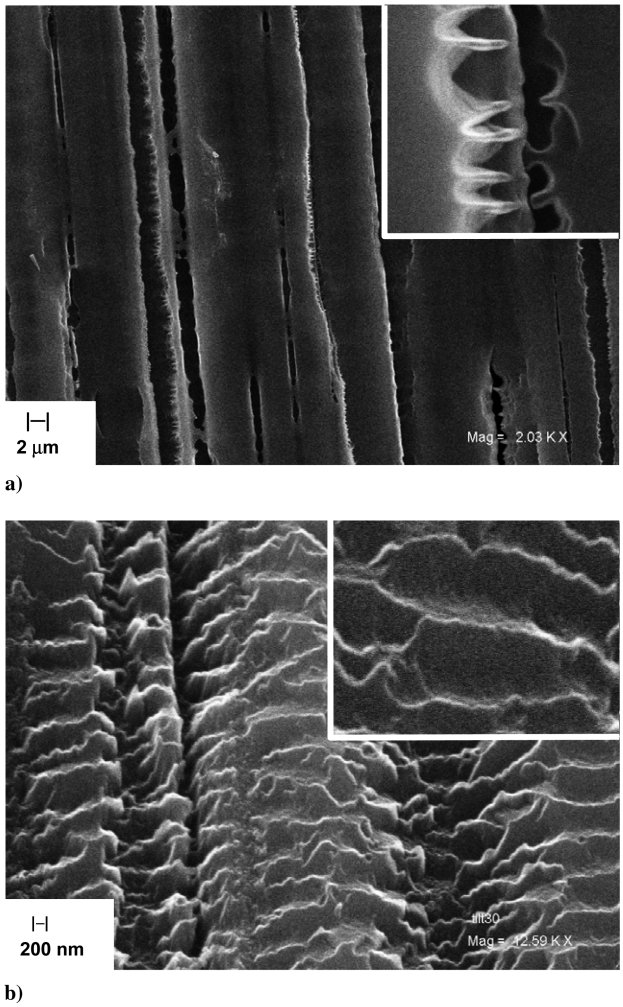

Fig. 7 SEM micrographs of CFC (KUP-VM) surface after 30 keV Ar^+ ion irradiation: a) RT and b) $T = 350$°C; inset magnitude is 2; $\varphi t \sim 10^{19}$ ion/cm^2.

relatively low temperatures ($T < T_a$), the fibers etching and formation of the troughlike longitudinal cavities are observed (see Figs. 7 and 8). It is interesting to note the nanoneedle formation on the cavity edges of the eroded fibers (Fig. 7a). The formation of the troughlike cavities is apparently due to different speeds of erosion of the fiber components: an imperfect kernel with a turbostratic structure and a perfect textured shell. At elevated temperatures ($T > T_a$), a crimped structure develops, with the ribs of the crimps perpendicular to the fiber axis (Figs. 7b and 8e). For KUP-VM, according to laser goniophotometry analysis, the crimp facet inclinations are ≈42° for N_2^+ and ≈23° for Ar^+ irradiation. One may suppose that the crimps developing as a result of physical sputtering of the mosaic structure of a perfect textured fiber shell at the conditions of radiation-defect dynamic annealing ($T > T_a$). The butt ends of the fibers are transformed into the craters (Figs. 8d and 8f), and such behavior is observed in all studied temperature range. It should be noted that under ion irradiation of Desna 4 (4-D), due to its specific architecture (three-dimensional reinforced orthogonal framework is complementary bonded by one of the diagonal), both the fibers on the sample surface and the fibers arranged perpendicularly to the sample surface are simultaneously irradiated.

B. Angular Dependences of Sputtering Yield Y

The experimental studies of angular dependences of sputtering yield $Y(\theta)$ on the angle θ of ion incidence, both for the polycrystalline graphites (till the temperatures at which radiation-enhanced sublimation begins) and for highly oriented pyrolytic graphite at $T < T_a$, are typical for physical sputtering of random solids [23]. Namely, as θ rises, sputtering yield increases according $Y \sim (\cos\theta)^{-1}$ up to $\theta_{\max}$ than Y decreases. It is confirmed by the comparison with the experimental results with the data simulated using TRIM.SP code both without (Fig. 9) and with (Fig. 10) taking into account developed surface topography [7,24,25]. Actually, the sputtering yields for polycrystalline graphites at temperatures higher than the temperature T_a for the given graphite do not differ from the values of Y at room temperature ($T < T_a$) within the measurement error. Quantitative differences in the $Y(\theta)$ dependences presented in Fig. 10 are mainly related to the differences in the topography developing under irradiation. For CFC KUP-VM, sputtering yields measured for

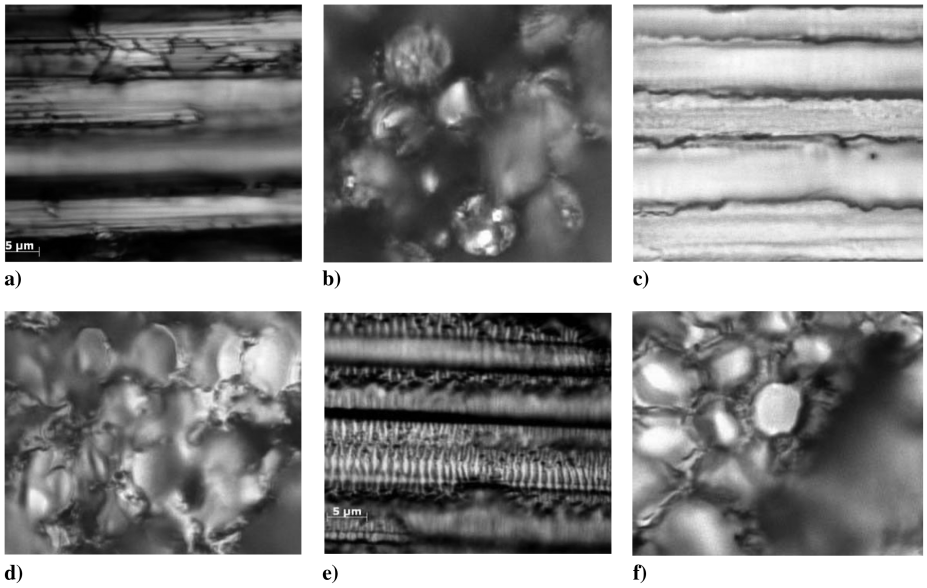

Fig. 8 Photographs of Desna 4 surface obtained by Axiostar Plus optical microscope: a–b) before and after 30 keV Ar^+ ion irradiation, c–d) RT, and e–f) $T = 350°C$; $\varphi t \sim 10^{19}$ ion/cm^2.

the samples cut both perpendicular to and parallel to the fiber directions are practically equal (Fig. 11) and close to data for polycrystalline graphites. The sputtering yields for 4-D reinforced-composite Desna 4 at ion fluence $\varphi t \sim 1 \times 10^{19}$ ion/cm^2 are close to the values for smooth graphite surfaces simulated using SRIM-2008. One may suppose that, in contrast to KUP-VM at the indicated fluence, the ion-induced topographic changes of Desna 4 surface are practically insignificant. As ion fluence rises, Y increases remain smaller than for KUP-VM (see Fig. 11).

Among carbon-based materials, HOPG has the highest degree of three-dimensional ordering. The density, crystal lattice parameters, preferential orientation in the 0001 plane, and anisotropy of physical properties of highly oriented pyrolytic graphite are closest to the natural graphite crystals. As in the natural graphite crystal, its structure is characterized by a carbon-atom arrangement in parallel layers; the atoms in each layer form a regular hexagonal network (see Fig. 1). It must be remembered that, according to the RHEED data, the tendency to more fully restore the UPV-1T structure is observed at elevated temperatures and grazing ion incidence. The behavior of the angular dependences of sputtering yield for the UPV-1T basal plane irradiated by 30 keV N_2^+ ions at elevated irradiation temperatures was found to be substantially different from the $Y(\theta)$ measured at RT (Fig. 12). It can be seen that the curve $Y(\theta)$ at $T = 400°C$ is nonmonotonic and indicates a wide and deep minimum at $\theta = 60°$. One can see that the sputtering yield decreases more than three times as compared to the case of irradiation at RT. This strong sputtering suppression is most likely related to the development of the specific surface relief with topographic elements in the form of needle-shaped cone elements (Fig. 4d). It is known that this topography promotes a decrease in the yield of sputtered atoms by virtue of the reflection of bombarding particles from steep walls of needle-shaped cones, whereas the secondary capture of particles prevents ejection of most atoms leaving the surface because of sputtering [15]. For the HOPG basal plane irradiated by 30 keV Ar^+ ions, sputtering-yield suppression (Y is twice as small) over all incidence angles (other than normal and near-normal angles), in comparison with polycrystalline graphites and glassy carbons, has been observed in all studied temperature ranges (Fig. 9). The possible

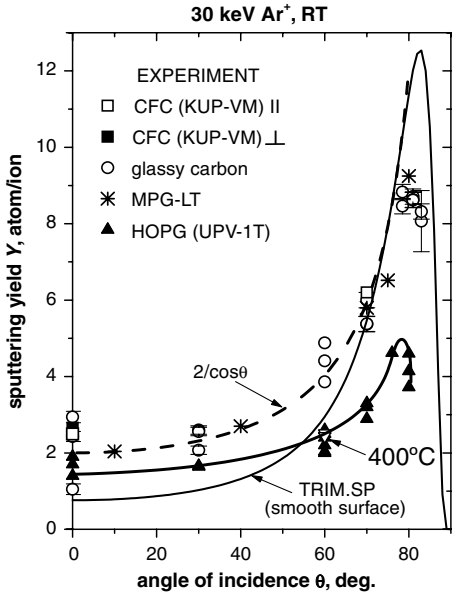

Fig. 9 Angular dependences of sputtering yield of carbon materials; data for MPG-LT are taken from [24], and simulated data are from [7].

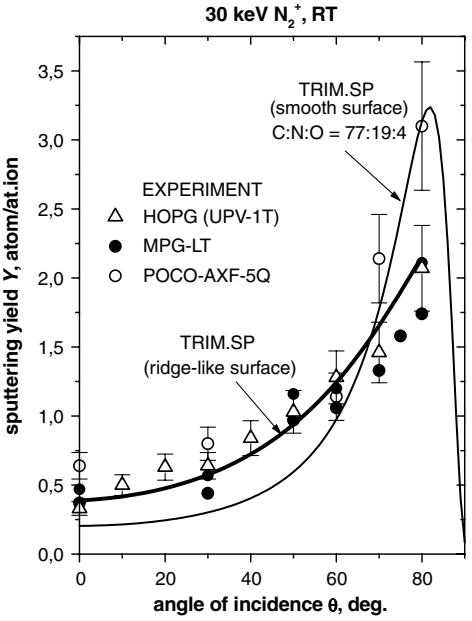

Fig. 10 Angular dependences of Y of the graphites irradiated at RT.

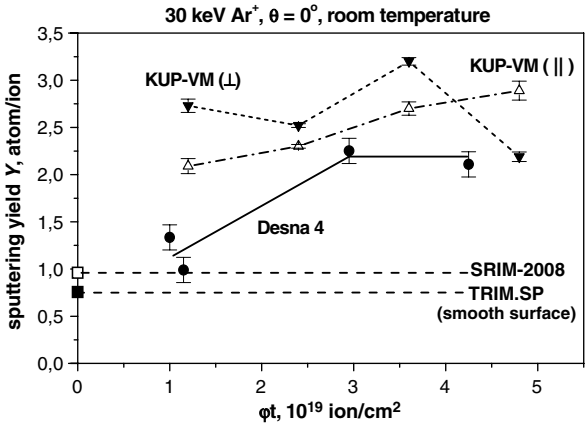

Fig. 11 Sputtering-yield dependences on irradiation fluence of carbon composite materials.

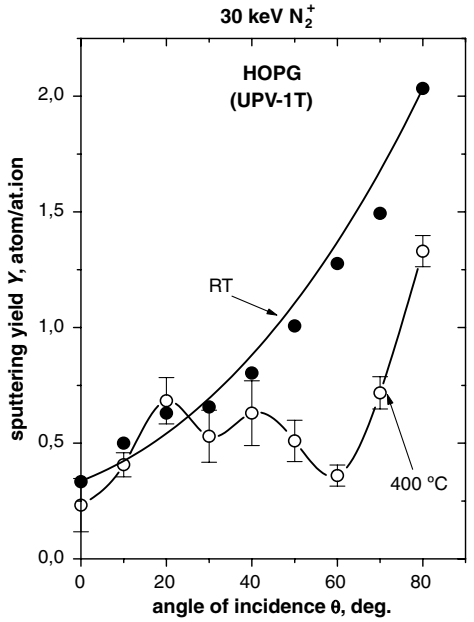

Fig. 12 Angular dependences of sputtering yield of the UPV-1T (0001) basal plane.

reason for it is an absence of full disordering under Ar^+ ion irradiation in the studied temperature range. Actually, at $T = T_t =$ 150°C, corresponding to the maximum of $\gamma(T)$ dependence, ion-induced texture transition takes place [26]. This is confirmed both in our RHEED studies (at $T < T_t$ the rings typical for polycrystal graphite phase are observed) and data discussed in [27]. As discussed above, the developed topographies (Fig. 5) are practically the same at RT and elevated temperatures and have a component consisting of accreted needle-shaped elements. As in the case of 30 keV N_2^+ ion irradiation at oblique ion incidence angles and $T > T_a$, the sputtering suppression in the case of 30 keV Ar^+ ion irradiation due to topography formation typical for ordered solids is caused mainly by the defect-diffusion roughening mechanism [6].

V. Conclusions

This paper focuses on the physical processes of high-fluence ion interaction with carbon-based materials, which are the background of the estimates devoted to material modification and radiation damage on long flights lasting many years in space.

The regularities of sputtering, structure, and morphology changes of the modified surface layers under high-fluence (tens of kiloelectron volts) heavy-ion irradiation of commercial carbon-based materials such as polygranular graphites, highly oriented pyrolytic graphite, glassy carbons, and carbon-fiber composites have been studied.

Ion-induced electron emission has been used as the effective tool for in situ monitoring of structural changes of carbon-based materials under ion irradiation. The regions of a different behavior of the irradiated material characteristics are separated by the dynamic annealing temperature T_a of radiation damage (or ion-induced texture transition temperature T_t), determined by a jump of an electron emission yield. In the studied case of Ar^+ ion irradiation of carbon-fiber composites $T_a \approx 170$°C is close to the corresponding values for polycrystalline graphites.

Strong dependence of the structure and surface morphology on ion irradiation temperature in the studied range from room temperature to 400°C has been found. At the conditions of radiation-defect dynamic annealing ($T > T_a$) the diffusion of the surface atoms may lead to strong and complex dependence of surface morphology on irradiation temperature. For highly oriented pyrolytic graphite the specific character of the developing topography (accreted needlelike cone elements) leads to a decrease in the sputtering yield by several times as compared to irradiation of other carbon-based materials. The crimps developing on the CFC fibers are possibly a result of physical sputtering of mosaic structure of perfect textured fiber shell.

For all studied carbon-based materials for N_2^+ ion irradiation, as for Ar^+, the angular sputtering regularities are typical for physical sputtering of random solids. Computer simulation of sputtering taking into account developed surface topography has satisfactorily agreed with the experimental data.

Acknowledgments

The authors are grateful to M. A. Timofeev for scanning electron microscopy analysis and E. A. Pitirimova for performing reflection high-energy electron diffraction. This work is supported by the Federal Agency of Science and Innovations (contract no. 02.740. 11.0389).

References

[1] Virgil'ev, Yu. S., and Kalyagina, I. P., "Carbon-Carbon Composite Materials," *Inorganic Materials*, Vol. 40, Suppl. 1, 2004, pp. S33–S49. doi:10.1023/B:INMA.0000036327.90241.5a

[2] Ehrhart, P., Schilling, W., and Ullmaier, H., "Radiation Damage in Crystals," *Encyclopedia of Applied Physics*, Vol. 15, VCH, New York, 1996, pp. 429–457.

[3] Burchell, T. D., "Radiation Effects in Graphite and Carbon-Based Materials," *MRS Bulletin*, Vol. 22, No. 4, 1997, pp. 29–35.

[4] Dienes, G. J., and Vineyard, G. B., *Radiation Effects in Solids*, Interscience, New York, 1957.

[5] Carter, G., "The Physics and Applications of Ion Beam Erosion," *Journal of Physics D: Applied Physics*, Vol. 34, 2001, pp. R1–R22. doi:10.1088/0022-3727/34/3/201

[6] Chan, W. L., and Chason, E., "Making Waves: Kinetic Processes Controlling Surface Evolution During Low Energy Ion Sputtering," *Journal of Applied Physics*, Vol. 101, 2007, Paper 121301. doi:10.1063/1.2749198

[7] Behrish, R., and Eckstein, W., (eds.), *Sputtering by Particle Bombardment, Experiments and Computer Calculations from Threshold to MeV Energies*, Springer, Berlin, 2007.

[8] Novikov, L. S., Panasyuk, M. I., and Voronina, E. N., "Space Model–A New Russian Handbook on Spacecraft/Environment Interaction," *AIP Conference Proceedings of ICCMSE*, Vol. 1087, 2009, pp. 637–644. doi:10.1063/1.3076879

[9] Mashkova, E. S., and Molchanov, V. A., *Medium-Energy Ion Reflection from Solids*, North Holland, Amsterdam, 1985.

[10] Borisov, A. M., Eckstein, W., and Mashkova, E. S., "Sputtering and Ion Induced Electron Emission of Graphite Under High Dose Nitrogen Bombardment," *Journal of Nuclear Materials*, Vol. 304, No. 1, 2002, pp. 15–20. doi:10.1016/S0022-3115(02)00871-1

[11] Andrianova, N. N., Borisov, A. M., Mashkova, E. S., Nemov, A. S., and Shulga, V. I., "The Effect of Microrelief Evolution on the Angular Dependence of Polycrystalline Cu Sputtering Yield," *Nuclear Instruments & Methods in Physics Research, Section B*, Vol. 230, Nos. 1–4, 2005, pp. 583–588.

doi:10.1016/j.nimb.2004.12.105
[12] Eckstein, W., *Computer Simulation of Ion-Solid Interactions*, Springer Series in Material Science, Springer, Berlin, 1991.
[13] Williams, J. S., and Poate, J. M. (eds.), *Ion Implantation and Beam Processing*, Academic Press, New York, 1984.
[14] Borisov, A. M., and Mashkova, E. S., "Ion-Induced Electron Emission from Carbon-Based Materials," *Nuclear Instruments & Methods in Physics Research, Section B*, Vol. 258, 2007, pp. 109–115. doi:10.1016/j.nimb.2006.12.078
[15] Behrish, R. (ed.), *Sputtering by Particle Bombardment II*, Springer, Berlin, 1983.
[16] Bacon, D. J., and Rao, A. S., "The Structure of Graphite Bombarded with Light, Gaseous Ions," *Journal of Nuclear Materials*, Vol. 91, 1980, pp. 178–188. doi:10.1016/0022-3115(80)90045-8
[17] Andrianova, N. N., Borisov, A. M., Mashkova, E. S., Nemov, A. S., Parilis, E. S., Sorokin, A. I., and Virgiliev, Yu. S., "Ion-Induced Electron Emission of Glassy Carbons," *Nuclear Instruments & Methods in Physics Research, Section B*, Vol. 256, 2007, pp. 515–519. doi:10.1016/j.nimb.2006.12.051
[18] Roth, J., Tsitrone, E., and Loarte, A., "Plasma-Wall Interaction: Important Ion Induced Surface Processes and Strategy of the EU Task Force," *Nuclear Instruments & Methods in Physics Research, Section B*, Vol. 258, 2007, pp. 253–263. doi:10.1016/j.nimb.2006.12.168
[19] Begrambekov, L., Brosset, C., Bucalossi, J., Delchambre, E., Gunn, J. P., Grisola, C., et al., "Surface Modification and Hydrogen Isotope Retention in CFC During Plasma Irradiation in the Tore Supra Tokamak," *Journal of Nuclear Materials*, Vols. 363–365, 2007, pp. 1148–1152. doi:10.1016/j.jnucmat.2007.01.147
[20] Novikov, L. S., Chernik, V. N., Naumov, S. F., Sokolova, S. P., Gerasimova, T. I., Kurilyonok, A. O., and Smirnova, T. N., "Degradation Testing of Spacecraft Materials for Long Flights in Low Earth Orbit," *Journal of Spacecraft and Rockets*, Vol. 43, No. 3, 2006, pp. 534–538. doi:10.2514/1.15661
[21] Ivanov, M. B., Gavrilov, N. V., Belyh, T. A., Ligacheva, E. A., Galijeva, L. V., Ligachev, A. E., and Sohoreva, V. V., "Irradiation Effects in Carbon Fibers After N^+-Ion Irradiation," *Surface & Coatings Technology*, Vol. 201, 2007, pp. 8326–8328. doi:10.1016/j.surfcoat.2006.12.034
[22] Andrianova, N. N., Borisov, A. M., Virgil'ev, Yu. S., Mashkova, E. S., Nemov, A. S., Pitirimova, E. A., and Timofeev, M. A., "Regularities of Ion-Electron Emission of One-Dimensional Carbon-Based Material," *Journal of Surface Investigation: X-Ray, Synchrotron and Neutron Techniques*, Vol. 2, No. 3, 2008, pp. 376–379. doi:10.1134/S1027451008030099
[23] Behrish, R. (ed.), *Sputtering by Particle Bombardment I*, Springer, Berlin, 1981.
[24] Mashkova, E. S., Molchanov, V. A., Fayazov, I. M., and Eckstein, W., "Experimental and Computer Study of Angle Dependences of Graphite Sputtering Yield," *Poverkhnost Fizika Khimiia Mekhanika*, No. 2, 1994, pp. 33–38 (in Russian).
[25] Borisov, A. M., Mashkova, E. S., Nemov, A. S., Kameneva, S. A., Kurnaev, V. A., and Trifonov, N. N., "Effect of Ion-Induced Relief on High-Dose Sputtering of Graphite," *Problems of Atomic Science and Techniques*, Thermonuclear Fusion, No. 2, 2004, pp. 65–72 (in Russian).
[26] Andrianova, N. N., Borisov, A. V., Mashkova, E. S., Parilis, E. S., Pitirimova, E. A., and Timofeev, M. A., "Monitoring the Structure-Phase Changes in Graphites Using Temperature Regularities of Ion-Induced Electron Emission," *Vacuum*, Vol. 84, No. 8, 2010, pp. 1033–1037. doi:10.1016/j.vacuum.2009.11.008
[27] Chernikov, V. N., Kesternich, W., and Ullmaier, H., "Radiation Effects and Gas Cavities in Pyrolytic Graphite Implanted with Helium Ions," *Journal of Nuclear Materials*, Vol. 227, 1996, pp. 157–169. doi:10.1016/0022-3115(95)00157-3

D. Edwards
Associate Editor